A new process chain for producing bulk metallic glass replication masters with micro and nano scale features

Pierre C. Vella[a, c], Stefan S. Dimov[a], Emmanuel Brousseau[b],, Ben R. Whiteside[d]

[a] *School of Mechanical Engineering, University of Birmingham, Edgbaston, Birmingham, B15 2TT, UK*

[b] *Cardiff School of Engineering, Cardiff University,Cardiff CF24 3AA, UK*

[c] *Department of Industrial and Manufacturing Engineering, University of Malta, Msida MSD2080, Malta*

[d] *The Centre for Polymer Micro and Nano Technology, University of Bradford, Bradford, West Yorkshire, BD7 1DP, UK*

Abstract

A novel process chain for serial production of polymer based devices incorporating both micro and nano scale features is proposed. The process chain is enabled by the use of Zr-based bulk metallic glasses (BMG) and thus to achieve the necessary level of compatibility and complementarity between its component technologies. It integrates two different technologies, namely laser ablation and focused ion beam (FIB) milling for micro structuring and sub-micron patterning, respectively, and thus to fabricate inserts incorporating different length scale functional features. Two alternative laser sources, namely Nanosecond (NS) and Picosecond (PS) lasers, were considered as potential candidates for the first step in this master making process chain. The capabilities of the component technologies together with some issues associated with their integration were studied. To validate the replication performance of the produced masters, a Zr-based BMG insert was used to produce a small batch of micro fluidic devices by micro-injection moulding. Furthermore, an experimental study was also carried out to determine whether it would be possible by NS laser ablation to structure the Zr-based BMG workpieces with a high surface integrity while retaining the BMG' s non-crystalline morphology. Collectively, it was demonstrated that the proposed process chain could be a viable fabrication route for mass production of polymer devices incorporating different length scale features.

Keywords: Laser Ablation, Focused Ion Beam Milling, Bulk Metallic Glasses, Process Chains, Function and Length Scale Integration, Micro-injection Moulding

1. Introduction

The global market for miniaturised products has been increasing continuously in the last decade . (HLG, 2011). This trend is a direct consequence of the growing needs and demands across a range of industry sectors (e.g. biotechnology, energy, medical, optoelectronics, micro-optics, printed electronics and ultra-precision engineering) to integrate multiple functionality in the smallest possible enclosures/packages by combining the latest advances in functional materials and high throughput micro and nano manufacturing technologies. In addition, the development of such multifunctional miniaturised products offers other important advantages, in particular significant cost, size, material usage and power consumption reductions.

Thus, it is not surprising that this trend for function integration in current and new emerging products has motivated researchers to look for new ways to "harness" the latest advances in functional materials and micro and nano manufacturing technologies and thus to create manufacturing capabilities for function and length scale integration (FLSI) at part and product levels (Bigot, Minev, Dimov, & Dobrev, 2011). These capabilities underpin the development of new miniaturised devices that depends on the manufacture of components incorporating functional features covering the whole range of sizes from few 100 μm to sub-100 nm**.** In addition, to achieve FLSI in a single part it is very important to explore the opportunities that new specially developed materials can offer and thus to benefit from their "optimised" properties for micro and nano scale processing (Dimov, Brousseau, Minev, & Bigot, 2012) .

Micro and nano manufacturing technologies that underpin the development of multifunctional miniaturised products are limited in their capabilities for producing structures with different length scale features cost effectively, from a few millimetres down to nanometres, in different materials (Dimov et al., 2012). Therefore, the capabilities of complementary and at the same time compatible manufacturing technologies are usually combined in process chains to produce miniaturised devices incorporating different length scale features. Such process chains can provide the necessary manufacturing solutions for achieving both high throughput and cost effective production of micro and nano structured parts and devices. So, the efforts of research groups and companies are focused on designing, validating and implementing processes and process chains that satisfy the specific

functional and technical requirements of new emerging multifunctional miniaturised products and thus to create the necessary pre-requisites for their scale up manufacture (Lalev et al., 2009; S. G. Scholz et al., 2011; Tosello, Bissacco, Tang, Hansen, & Nielsen, 2008; Velkova et al., 2011).

The integration of complementary and compatible technologies into process chains has been attempted before in developing promising micro manufacturing platforms (Dimov et al., 2012)**.** However, there are many important factors and processing constraints that need to be considered when combining and integrating micro and nano fabrication technologies. Therefore, it is really a challenging task to design and implement successfully process chains aiming at FLSI in innovative miniaturised products. In particular, it is necessary for the interfaces between component manufacturing technologies in the process chains to be analysed systematically in terms of their Capabilities, Complementarities and Compatibilities (C3), and this represents an important pre-requisite for their successful design and implementation.

A systematic study of technological interfaces between micro and nano fabrication technologies conducted by the authors revealed that the material of the workpiece plays a very important role in their successful integration and also in achieving FLSI in parts or replication masters (Minev, Vella, Brousseau, Dimov, Minev, et al., 2010; Minev, Vella, Brousseau, Dimov, Scholz, et al., 2010; Vella, Brousseau, Minev, & Dimov, 2010). Hence, when designing such chains it is necessary to utilise materials that facilitate the integration of the considered component manufacturing technologies, and at the same time satisfy the functional and technical requirements of the final product or master. For instance, to combine successfully the capabilities of two micro and nano structuring technologies, e.g. focused ion beam (FIB) machining and laser ablation, it is necessary to select a workpiece material with a favourable processing response to both technologies and also to take into account their respective constraints in producing different length scale features with the required surface integrity (Li, Minev, Dimov, & Lalev, 2007; Quintana, Dobrev, Aranzabe, Lalev, & Dimov, 2009; Vella et al., 2010).

The paper presents an experimental investigation of a process chain that is enabled by the use of a bulk metallic glass (BMG) as a workpiece material that combines the capabilities of the laser ablation and FIB machining technologies in producing replication masters incorporating micro and nano scale structures. To demonstrate its viability a mould insert was fabricated and then used to

produce a batch of polymer parts by micro-injection moulding. Such a process chain can be used for mass production of polymer parts incorporating different length scale features.

The paper is organized as follows. Section 2 discusses generic process and material related issues that have to be considered in achieving length scale integration in master-making process chains. It also provides an overview of the component technologies investigated this research. Then, Section 3 describes the experimental set-up employed to validate the capabilities of the proposed process chain. Finally, the obtained results are presented and discussed, and conclusions are made.

2. Process Chain Design

When designing process chains it is necessary to take into account the technical requirements of the product or replication master together with the processing constraints of their component micro and nano manufacturing technologies. Also, as it was already stated, the selection of a suitable workpiece material to facilitate the integration of these technologies into a process chain is an important factor in producing parts or replication masters with different length scale functional features. Specifically, the microstructure and properties of a workpiece material need to be considered as one more “variable” in optimising the process chains, and thus to achieve a suitable level of C3 between the component fabrication technologies. The selected material should have a microstructure that is optimised for performing processing both at meso/macro and micro/nano scales. In particular, the micro or nano structuring response is favourable if, such a material is homogeneous and inclusion free at the considered processing scales. Thus, the material microstructure and properties of the workpiece are a critical factor affecting the machining results and their consistency in micro and nano manufacturing. Therefore, it is even more important when designing process chains aiming at FLSI in replication masters to identify suitable combinations of complementary structuring technologies and a workpiece material with a favourable machining response to them.

2.1 Process and Material Issues

Major advances in material processing technologies and especially in the development of amorphous coatings and alloys have attracted a considerable interest in recent years. This is due to the fact that the high hardness, fracture toughness and fatigue strength of such materials represent important value-added properties in a number of engineering applications (Inoue, 2000; Zhang, Liu, & Zhang, 2006). For example, amorphous coatings are advantageous for manufacturing micro-electro-mechanical systems (MEMS) and micro-sensor systems (Wang et al., 2007). Additionally, due to absence of any long range atomic order, lattice defects and grain boundaries (Kawasegi et al., 2006), amorphous metallic alloys are considered promising materials for micro and nano- structuring of replication masters (Minev, Ilieva, Kettle, Lalev, Dimov, et al., 2010; Quintana et al., 2009). The absence of grain boundaries in BMG makes them mechanically and chemically homogeneous for processing at all length scales down to a few nanometres. As a result, they are one of the preferred materials for micro- and nano structuring (Loffler, Kundig, & Dalla Torre, 2007). However, to benefit from their outstanding properties and employ them successfully in different application areas, it is of prime importance to maintain their non-crystalline morphology during machining, especially when producing parts incorporating micro- and nano-scale features (Quintana et al., 2009). In a recently conducted feasibility study, it was shown that the processing of an amorphous Nickel-based alloy workpiece with both nano-second (NS) and pico-second (PS) pulsed laser ablation did not trigger phase transitions in the material (Quintana et al., 2009). In particular, the reported research revealed that machining with both laser ablation regimes did not lead to any crystallisation and long-range atomic ordering of Ni-based metallic glasses. Additionally, there were no signs of crack formation, which indicates a preserved surface integrity after laser machining with short- and ultra-short pulses. Another study reported the effective machining of Mg-based BMG using a 355nm pulsed NS laser. In this study it was demonstrated that by an appropriate adjustment of the laser parameters the non-crystalline morphology of the Mg-based BMG was preserved (Lin, Lee, Hu, Li, & Huang, 2012). Hence, both PS and NS laser machining regimes should be considered as very promising methods for the cost effective micro structuring of metallic glasses.

Another study which compared the machining response of an amorphous and polycrystalline Ni alloys when subjected to FIB milling, showed that a higher surface integrity could be achieved when

processing the amorphous Ni-based BMG under identical conditions to those used for the polycrystalline Ni alloy (Li et al., 2007).

Thus, laser ablation in NS and PS regimes and FIB milling satisfy the C3 prerequisite for their integration in process chains and are promising combinations of complementary technologies for structuring BMGs at micro and sub-micron length scales respectively without introducing any changes in their non-crystalline morphology. In particular, the potential integration of PS laser ablation and FIB machining in a process chain reported in a feasibility study (S. Scholz et al., 2009) suggested that PS laser ablation can be used for cost effective micro structuring of large areas on replication masters while FIB milling can be utilised to machine on a pre-existing topography very complex micro and sub-micron 2.5D and 3D structures. The same rationale also applies to the combination of NS laser ablation and FIB milling in a process chain. Thus, the component processes in such process chains can be utilised in their cost effective processing windows and complement each other in achieving FLSI in replication masters.

In the proposed master making process chains that are enabled by the use of a BMG as a workpiece material, first laser ablation is employed to structure relatively big surface areas with meso and micro scale resolution and acceptable surface integrity, and subsequently FIB milling is applied to achieve high resolution sub-micrometre and nano patterning within a relatively small field. In this manner, by combining the capabilities of these two complementary technologies it is possible to achieve cost effective FLSI in replication masters and benefit from the BMG' s superior mechanical properties for micro injection moulding (μIM) of thermoplastic polymers. A more detailed description of the capabilities of these component technologies in the proposed master making process chains is provided in the following sub-sections.

2.2 Laser machining

Laser micromilling as a technology for manufacturing replication masters has attracted research (Dobrev, Dimov, & Thomas, 2006; Petkov, Dimov, Minev, & Pham, 2008; S. G. Scholz et al., 2011) and industrial interest (M. Knowles, Kearsley, & Karnakis, 2007). Laser milling can be used to structure parts in a wide range of materials directly from CAD data via a layer by-layer machining

strategy (Pham, Dimov, Ji, Petkov, & Dobrev, 2004). Material removal occurs as a result of laser irradiation and depending on the laser source and the workpiece, the ablation can take place through melting and ejection or sublimation (Petkov, Dimov, et al., 2008). The process allows parts with complex shapes to be produced without the need for expensive tooling. Laser milling is mostly used for machining parts from one side only. However, complete laser milling of parts is also possible, but it is necessary to address the accuracy issues associated with the re-positioning of the workpiece, which are common process design concerns when more than one machining setup is necessary (Pham et al., 2004).

To set up the laser milling process and achieve the required surface integrity it is usually necessary to take into account a range of factors that can influence the machining outcomes (Pham, Dimov, & Petkov, 2007)**.** These include laser processing parameters and applied machining strategies(Fleischer & Kotschenreuther, 2007; Lalev et al., 2009; Petkov, Dimov, et al., 2008; Uriarte et al., 2006; B. Wu & Ozel, 2011). Thus, their interdependencies and effects on different output characteristics such as the achievable surface integrity or the material removal rate have to be studied systematically in order to identify optimum processing windows. Short, NS, and ultra-short laser sources, femtosecond (FS) and PS, have many applications in micro-machining of metals, semiconductors, and dielectrics for the fabrication of electronic, medical, optical and other devices(B. Wu & Ozel, 2011). The ultra-short lasers have the advantage of extremely high radiation intensities and thus can ablate almost any material with minimal and sometimes even negligible heat affected zone and therefore they are used for precise material removal (Brousseau, Dimov, & Pham, 2010; B. Wu & Ozel, 2011).

NS laser technology is mature and is widely adopted in industry for micro machining (M. R. H. Knowles, Rutterford, Karnakis, & Ferguson, 2007). This is largely due to their cost-effectiveness and reliability and therefore NS lasers are used in many industrial applications. A major advantage of NS laser ablation is their achievable higher removal rates when compared to lasers with shorter pulses (Quintana et al., 2009).

However, micro machining can be a challenging application for NS lasers. Good quality sidewalls can generally be obtained, but it is usually very difficult to achieve the necessary surface integrity for some applications, e.g. replication masters (M. Knowles et al., 2007). The ultra-short lasers, FS and PS, have a number of advantages in micro machining. The very high repetition rate of the latest generation of FS and PS laser sources together with the advances in the scanning heads' technology allow the resulting surface integrity to be improved substantially while maintaining a higher processing speed (Fleischer & Kotschenreuther, 2007; Petkov, Dimov, et al., 2008). However, it is worth noting that such improvements are at the expense of the removal rates when NS and PS laser machining results are compared.

Apart from micro machining, lasers are also used for surface texturing (Bonse, Kruger, Hohm, & Rosenfeld, 2012; Etsion, 2005). Especially, they are applied for functionalising surfaces, e.g. to regulate cell-implant interaction for biomedical engineering applications (Vehse, Lobler, Schmitz, & Seitz, 2012), to reduce the surface friction in mechanical devices (Chen et al., 2012)**,** to modify the wetting properties of the surfaces (Fadeeva et al., 2011; P. H. Wu, Cheng, Chang, Wu, & Wang, 2011) , or to reduce the surface reflectance (Nayak & Gupta, 2010). Such applications are also very interesting for master making as laser surface texturing rates are still low for cost effective direct structuring of parts with relatively large surface areas.

In this research, the choice of the laser source requires careful consideration in order to avoid any detrimental effects on the non-crystalline morphology of the BMG workpiece. Such effects are of a particular importance for the proposed process chain as any phase transformations or crack generation will not only change the material properties of the replication master but can also affect any subsequent sub-micron structuring by FIB milling. Therefore, two alternative laser sources were considered as potential candidates for the first step in this master making process chain. The primary focus of the research is on investigating the feasibility of utilising PS laser machining in the proposed master-making process chain due to its capabilities for machining accurately micro features whilst preserving the mechanical properties and surface integrity of the workpiece material. However, it is also possible to optimise the NS laser ablation process and achieve a relatively good surface integrity while benefiting both from the higher material removal rates and the superior mechanical properties of

BMGs as they can also be preserved during the processing with short pulse lasers. Therefore, it was also considered important to investigate the NS laser ablation of BMGs as an alternative component technology in the process chain, in particular what level of surface finish can be achieved without triggering any crystallisation.

2.3 FIB milling

The second stage in the process chain is FIB machining of sub-micron and nano-features over the pre-existing topography generated by laser ablation. The FIB milling process offers many advantages, such as flexibility, high resolution and high surface quality that are extremely important for master making (S. Scholz et al., 2009; Youn, Takahashi, Goto, & Maeda, 2006).

The input data for FIB milling can be in a bitmap format when it is necessary to produce simple features like 2.5D channels. In this case, the data can be uploaded into most FIB systems directly. Then, the built-in pattern generator of such systems is used to create directly the 2.5D features. A more sophisticated approach to 2.5D feature generation requires the use of a lithography software and hardware like Elphy Quantum (Raith GmbH) or Nanomaker where various 3D shapes can be designed, duplicated, and if necessary the respective exposure doses specified. However, the generation of complex 3D shapes like diffractive optical elements, necessitates a different data preparation procedure. Such 3D structures can be designed by employing any 3D CAD package and then, by following a sequence of data translation operations, the 3D geometry is converted into a stack of layers ordered along the vertical axis of the 3D model (Lalev, Dimov, Kettle, Van Delft, & Minev, 2008). After such a 'slicing' step, the model is exported into a GDSII stream file format and each GDSII layer represents a set of exposure pixels defining a slice of the model at a given point along its vertical axis.

The main FIB parameters that should be considered when optimising the process are: ion beam current, ion beam fluence, and exposure time (Lalev et al., 2008; Li et al., 2007; Minev, Ilieva, Kettle, Lalev, Dimov, et al., 2010; Velkova et al., 2010). An ion beam sputtering simulation software can also be employed to predict and thus reduce some negative effects such as re-deposition of sputtered material and over-etching (Svintsov et al., 2009). Its use as a data pre-processing step before FIB

milling makes it possible to optimise the process parameters and even to modify the model in order to counteract material re-deposition effects (Velkova et al., 2010) .

Another important issue when structuring processes are integrated in process chains is the alignment of new features to any pre-existing features/topography on the workpiece. In the proposed chain, this alignment could be realised either by manually positioning the sample stage while inspecting the specimen in SEM or FIB imaging modes, or automatically, by using the ‘‘feature recognition” option available in some FIB systems to find alignment marks machined in the preceding processing steps.

As stated previously, the main disadvantage of the FIB milling technology is its relatively low removal rates. Consequently, to address this issue and thus to be able to nano structure larger areas, a multi-ion beam concept was proposed that combines the high resolution capabilities of the FIB technology with the high throughput that parallel lithography systems can offer. In particular, to satisfy the requirements for high productivity, a projection maskless nano-patterning (PMLP) system has been developed (Platzgummer, Loeschner, & Gross, 2008). A prototype, which incorporated 48,000 beams working in parallel, demonstrated a significant increase of the removal rates and improved resolution compared to conventional single FIB systems.

2.4 Micro Injection Moulding

The proposed master-making process chain can be used to produce masters for scale-up micro replication including µIM and hot embossing (HE) (Heckele & Schomburg, 2004). In particular, µIM and HE can process any thermoplastic polymer and are considered important technologies for the cost effective serial fabrication of micro-parts (Giboz, Copponnex, & Mele, 2007). HE is widely used for replicating structures with dimensions in the sub-micron range and with high aspect ratios. The process is very effective for producing such functional features and can minimise the stress induced birefringence due to the very low flow rates of the material in the imprinting plates. However, HE cycle times, which are usually in the range from 5 to 10 minutes, are relatively long and therefore this

technology is more suitable for small to medium series production and prototyping (Giboz et al., 2007; Heckele & Schomburg, 2004) . Conversely, the shorter µIM cycle times, which are in the order of seconds makes it effective for high volume production with low production costs per part once the process has been properly configured. Given that the development of new micro devices is highly dependent on manufacturing systems that can reliably and economically produce micro parts in large quantities, it is clear that µIM provides a more attractive option. Therefore, in this study, the structured BMG inserts was used as a master for µIM in order to validate the proposed process chain.

When replicating micro and nano-structures employing µIM, the accuracy of the mould masters is an important prerequisite. Nonetheless, the complex flow and cooling behaviour of the thermoplastic materials can also have a significant influence on achievable product quality. It is therefore usually necessary to optimise the µIM process using design of experiments (DOE) approaches. There are numerous parameters which can influence the process but the most statistically significant factors (Attia, Marson, & Alcock, 2009; Giboz et al., 2007; Griffiths, Dimov, Brousseau, & Hoyle, 2007; Sha, Dimov, Griffiths, & Packianather, 2006) include: melt temperature; mould temperature; injection speed; holding pressure and duration; mould surface roughness; runner and gate design and venting/ vacuum systems.

Micro-moulding geometries typically have a very high surface to volume ratio when compared with macro scale injection moulded products, which means that polymer solidification can be very rapid, with cooling rates in a fraction of a second in many cases. Such conditions require short filling times to ensure the temperature of the material does not fall below the no-flow temperature before the mould is completely filled. The heat flow during solidification can also have a significant influence on the internal morphology of the part and also on a range of properties affecting its mechanical behaviour. Therefore, the thermal behaviour of the polymer-mould system can have a high impact on the final product's properties and therefore a very accurate control of the melt and mould temperatures is required to achieve a stable process. As a consequence the µIM process windows for quality components tend to be much smaller than those in conventional injection moulding. In particular, any small changes in the parameter settings can shift the process outside these small windows with detrimental effects on part quality. It is therefore very important to optimise the µIM process for the particular polymer in use and thus to ensure a stable and reliable micro replication process.

3. Experimental Setup

3.1 Insert Material

The BMG used in this study was a Zr-based BMG, namely Vitreloy 1b (Vit1b). The mechanical properties of this alloy are particularly attractive for the fabrication of high wear resistant mould inserts for µIM, especially its high tensile yield strength, 1.9 GPa, and high hardness, 540 Hv. Furthermore, it is expected that micro and nano-structures machined in this material will have a high level of surface integrity due to the fact that crystalline defects, such as dislocation pile-ups, point defect agglomerates and grain boundaries, are not present in the material. Using wire electro discharge machining, the Zr-based BMG sample was cut to produce a circular workpiece with a thickness of 3 mm and a diameter of 10 mm.

3.2. Test Structure Design

The 2D design of a Quick Response (QR) code is used as a test structure.

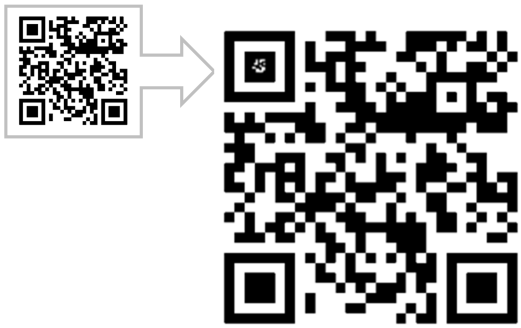

Fig. 1 Bitmap images of the QR code

The QR code is a specific matrix barcode that consists of square fields in black colour on a white background. The information encoded by such patterns can represent text or other data. The specific QR code used is shown in Fig. 1 and it consists of 29 x 29 black or white squares. This pattern was machined at two different length scales on the BMG workpiece. First, a micro scale pattern of the QR

code was produced using laser ablation. At this scale, each square has a width of 75 µm and the white squares correspond to pockets with a depth of 10 µm. Next, a nano-scale version of the code was machined on top of a micro-scale black square, as shown in Fig. 1, using FIB machining. In this scale, each square has a width of 2.59 µm and the white squares correspond to pockets with a depth of 900 nm. This test structure was selected to demonstrate the feasibility of incorporating different length scale features, micro and sub-micron, cost effectively into replication masters for anti-counterfeiting purposes. In particular, such QR codes could be replicated on the surfaces of macro and meso scale polymer parts.

3.3 Laser Ablation

As it was stated in Section 2.2, PS and NS laser ablation can be used for micro machining of BMGs without triggering any crystallisation. Therefore, in this research two different laser systems were utilised to investigate laser-BMG interactions in these two ablation regimes.

The PS laser ablation is used for machining the features of the micro-scale QR code on the BMG workpiece. To perform laser structuring, first the bitmap file of the QR code was converted into a .dxf (Drawing Interchange Format) format, and then the model was scaled to ensure that the square fields are machined to the specified sizes of 75 µm x 75 µm. Next, this data file was used to generate the laser machining path. A layer-based machining strategy was selected for this study. In particular, the strategy included random “hatching” with a step over of four micrometres between the parallel passes of the laser beam and this was then followed by a border cut for each layer (Petkov, Scholz, & Dimov, 2008). The PS laser ablation system used to perform this laser structuring operation incorporates a mode-locked Nd:YVO4 green (532 nm) laser source. The process settings used to carry out the PS laser machining are provided in Table 1. The process settings were selected in such a way so that in parallel to the machining of the QR code, the machined fields were also textured with self-organised structures and thus to investigate the µIM capabilities when replicating surfaces with a wide range of micro and sub-micron features/structures.

Table 1: PS laser parameters

Pulse duration	8 ps
Repetition rate/ Pulse frequency	50 kHz
Laser beam scanning speed	10 mm/s
Power	25 mW
Fluence	0.28J/cm^2
Pulse energy	0.5 µJ
Hatch distance	4 µm
Beam quality	M^2<1.3

In addition, an experimental study was carried out to determine whether it would be possible by NS laser ablation to structure Zr-based BMG workpieces with a high surface integrity without triggering any crystallisation. A system that integrates a NS near infrared fibre laser was used to machine fields with depth of approximately 20 µm. Some initial trials were conducted with different processing conditions, in particular by varying scanning speed, pulse duration, repetition rate and fluence, to identify combinations of processing parameters for achieving a high surface integrity with a minimal thermal load. Based on these trials the process settings in Table 2 were selected as promising for achieving high surface integrity with minimal thermal damage. Using these settings 10x10 mm fields were laser machined on three Vit 1B samples for a X-ray diffraction (XRD) analysis. After completing the NS laser machining, the three samples were ultrasonically cleaned with a light degreaser to remove any debris without affecting the resulting surface roughness. It should be stressed that this was just a feasibility study to determine whether it will be possible by NS laser ablation to achieve a high surface integrity while retaining the BMG non-crystalline morphology.

Table 2. NS-Laser Parameters

Sample	Pulse Frequency [kHz]	Average Power [W], (measured)	Pulse energy [µJ]	Fluence [J/cm^2] @ 35 micron spot	Pulse duration, [ns]	Scanning speed V [mm/s]	Track distance, [µm]	Layer thickness [µm]	Hatch direction
1	40	0.72	18	1.87	220	600	15	1	cross, 90°
2	250	1.45	5.8	0.60	25	1000	6	0.15	random
3	40	0.72	18	1.87	220	200	5	0.3	random

3.4 FIB Processing

The next process in the proposed chain was FIB milling of the features with nanometre depth over the micro-topography produced by laser milling. The nano-scale QR code was machined on the BMG workpiece using a Carl Zeiss XB 1540 FIB/SEM system that combines a gallium ion beam with an electron beam column. As it was mentioned earlier, the FIB milling process can be controlled by utilising a built-in software or an external nanolithography system (Lalev et al., 2008). Given that the QR code represents a 2D image composed of black and white fields/pixels, the bitmap file of this pattern was processed directly by the built-in software of the FIB system to control the milling operation. The depth and accuracy of the structures fabricated by FIB milling are determined by the processing parameters used. In this study, the process was set up and optimised by conducting trials to find a suitable processing window and thus to achieve the best trade-offs between machining time and feature quality. Especially, in identifying the process parameters it was taken into account that FIB milling with low current results in a better pattern resolution but at the expense of longer milling times. It should also be noted that by increasing the processing time the possibility for quality deterioration and pattern drift also increases. The FIB milling parameters used in this study are provided in Table 3. The alignment of the nano-scale QR pattern over the micro-scale code was performed by a manual stage control with the help of the FIB imaging mode of the system.

Table 3: FIB parameters

Probe current	200 pA
Accelerating voltage	30kV
Exposure time duration	3 hours
Probe size	40 nm

3.5 Micro Injection Moulding

The machine used to perform the µIM trials was a Battenfeld Microsystem 50 with a 5 mm diameter injection plunger. The BMG insert was integrated into a larger circular cavity mould and installed into a modular tool assembly based on a Hasco 95mm x 95mm standard. The cavity form is a disc with a 17 mm diameter and 0.5 mm depth. The tool is thermoelectrically heated using a cartridge heater array and temperature control was performed using the integrated control system in the machine. Images in Figure 2 depict the assembled mould and one of the replicas.

(a) Mould assembly (a) µIM part

Fig. 2 Images depicting the assembled mould and one of the replicas.

A material commonly used in injection moulding for optical devices, namely Cyclic Olefin Copolymer (COC) with a trade name Topas 5013S was selected to conduct the replication trials.

Before the experiments, the polymers were placed in industrial desiccant dryers for four hours at the manufacturers recommended drying temperatures to remove any moisture.

To fill completely a mould cavity that incorporates micro and sub-micron features it is very important to select the right processing window. Taking into account the results of other experimental studies (Huang, 2007; Monkkonen et al., 2002; Sha et al., 2006; Tosello, Gava, Hansen, & Lucchetta, 2010), some preliminary trials were conducted to identify an appropriate combination of parameter settings and thus to produce replicas of required quality.

The trials showed that the mould temperature had the highest influence on the replication quality. Therefore, a set of experiments were subsequently performed with the mould temperature settings in Table 4 in order to investigate the influence of mould temperature on the replication fidelity in terms of feature width, depth and shape. These settings were selected based on the material manufacturer's data sheets, experimental investigations reported in literature, and the performed trials.

To obtain representative results, the µIM process was first allowed to stabilise for each set of process parameter settings by producing at least 40 components and then a small batch of parts was produced for quality assessments.

Table 4: Process Settings for Micro-Injection Moulding Trials

Trial No / Parameters	1	2	3	4	5
Melt temp -- T_b [^oC]	290	290	290	290	290
Mould Temp -- T_m [^oC]	80	110	115	130	140
Holding Pressure -- P_h [Bar]	1300	1300	1300	1300	1300
Injection Speed -- V_i [mm/s]	200	200	200	200	200

3.6. Inspection

The surface integrity and dimensional compliance to technical requirements of the tool and subsequently the replicas have to be assessed. Thus, a detailed dimensional analysis was carried out based on five key representative dimensions of both the laser and FIB machined QR codes on the

BMG insert and their corresponding polymer replicas. In particular, the widths and the heights/depths of the smallest features and the overall size of the codes were measured. The equipment and the respective inspection procedures employed in this research are described below.

3.6.1 Scanning Electron Microscope

SEM images of the QR codes were taken at each stage of the process chain in order to assess lateral (XY) and vertical (Z) dimensions of the produced parts. One BMG master was used for the detailed dimensional analysis. Ten “pixels” located in the corners and the centre of both the “large” and “small” QR codes were measured in X and Y respectively to obtain the width values of the smallest features. Whilst to obtain the values of the overall QR codes’ dimensions, five measurements were conducted along the X and Y axes. All X and Y measurements were carried out using the SEM. For the height/depth measurements of the smallest features, 10 “pixels” of the “large” QR code were measured. These Z measurements were carried out at an angle of 54^{o} between the electron beam and the sample holder. The tilt compensation option of the SmartSEM software was used to calculate the actual values of the vertical dimensions. For the polymer parts’ analysis, five replicated Topas samples were selected and each part was measured in the same way as the BMG insert.

3.6.2 Atomic Force Microscope

A representative area of the FIB milled and replicated small scale QR code was inspected with an atomic force microscope (AFM), Asylum Research MFP 3D, to judge about the FIB structuring and the µIM replication quality. The measurement was carried out when the instrument was in its tapping mode configuration. The probe used was parabolic in shape, with an apical tip radius of 15nm and a half cone angle (a) of 30°, from the vertical plane. The profiles of the features were obtained at the same place on the FIB milled insert and all µIM parts. For the mouldings, three samples were randomly selected from each batch of Topas 5013X parts. The dimensions of the scanned area were 50 x 50 µm. After the measurement, the data sets were processed using IGOR Pro 6 software in order to generate the average line profiles of the features and carry out on them depth and width

measurements. Finally, the average profiles for each batch produced were compared to decide which combination of process parameters gave the best replication results.

3.6.3 Confocal microscopy

The laser and FIB patterns on both the insert and mouldings were inspected using an Olympus LEXT 4000 laser scanning confocal microscope. Two modes of operation were used, in particular a 20× objective with a 25 image stitched dataset (5 horizontal, 5 vertical) for the large-scale QR code pattern and a single 100× image for the FIB structures.. The resolution of each image was 1024 x 1024 pixels and the overlap area for the stitching was 20%.

The surface roughness of the textured surfaces of the large scale QR-code on both the insert and the replicas together with the pixel step height measurements of the insert's "small" QR code were carried out using this confocal microscope. In particular, in order to determine the step heights, the integrated Olympus software was employed to obtain histograms of the height distributions. .Average step heights of the scan areas were determined by computing the difference between the individual mean heights of the histograms' two peaks as shown in Fig 3. For the polymer parts' dimensional analysis, five Topas replicas were measured in the same way as the BMG insert.

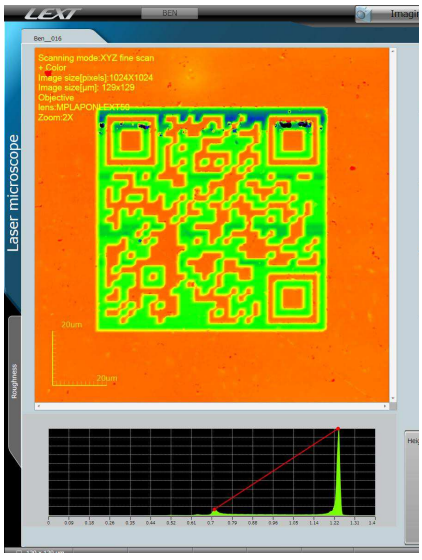

Fig 3 . Step Height Measurement Using Olympus Software

This method for evaluating average step heights was validated using a Veeco SHV2119 step height calibration artefact where 5 measurements were performed at various locations on the sample using the magnification parameters adopted for each scan. The results fell within the ranges defined by the calibration certificate so it was accepted as a valid technique.

For assessing the replication quality of the FIB structures on the BMG insert and five Topas replicas from each mould temperature setting, three methods were used:

i) *Volume ratio.* The volume of the features and cavities was determined using the LEXT software by considering the volume enclosed by the measured surface and a plane coincident with the original (pre-machined) surface. A ratio of the volume of the moulded feature relative to the original cavity volume was used as a measure of the replication quality.

ii) *Sa ratio*. The Sa parameter is the arithmetic mean of the absolute value of the height within the sampling area. The Sa parameter of both the features and cavities was determined using the LEXT software. The ratio between Sa of the moulded feature relative to the original cavity Sa was used as a measure of replication quality.

iii) *Average step height ratio*. As described earlier, the average step height was determined for the insert and each of the moulded specimens by using histogram information as shown in Fig 3. The ratio between the average step height of the moulded feature relative to the original cavity step height was used as a measure of replication quality.

3.6.4 XRD

The focus of the NS laser machining trials was to achieve as high as possible surface integrity without triggering any crystallisation and thus to preserve the attractive mechanical properties of Zr-based BMGs. Therefore, a XRD analysis of Vit 1B samples before and after laser machining to form 10x10 mm fields, was carried out using a Bruker D8 Advance' X-Ray Diffractometer with Ni filtered CuKa radiation to verify the amorphicity or otherwise of the four samples.

3.6.5 Talysurf 120L

The roughness measurements for the three NS laser machined samples were taken using a Talysurf 120 L surface texture measurement instrument. The sizes of the sampling/evaluation lengths were chosen according to ISO 4288:1997 (ISO4288, 1997). The parameter used to evaluate the surface roughness was the arithmetic mean roughness (Ra) because relative heights in microtopographies are more important, especially when measuring flat surfaces.

3.6.6 Dimensional and Surface Roughness Measurements Uncertainty

The average values of dimensional measurements were calculated and where deemed applicable were also provided with their associated expanded uncertainty, U, (at 95% confidence level) which was determined, following an established procedure (Joint Committee for Guides in Metrology (JCGM), 2008; Kirkup & Frenkel, 2006; United Kingdom Accreditation Service (UKAS), 2007).

The error sources for the SEM and confocal microscope were identified by adapting the recommendations given in literature for SEM and other non-contact measuring systems (Tosello & Chiffre, 2004; Tosello, Hansen, & Gasparin, 2009; Tosello, Marinello, & Hansen, 2012; Tosello, 2008; Velkova, 2011). In the case of the SEM, to account for the worst-case scenario the measurement uncertainty u(P) of the SEM measurements was calculated as 3% of the measurand's average value (Velkova, 2011)**.** The reported average surface roughness measurements are also provided with their associated expanded uncertainty, U, (at 95% confidence level) which was determined by following an established procedure (Leach, 2001) and by adapting recommendations given for surface roughness measurements in a separate study (Tosello et al., 2012)**.**

4. Results and Discussion

This section discusses the results obtained after each process step and includes the detailed dimensional analysis of the QR codes' micro and sub-micron structures.

4.1 Laser Milling

4.1.1 PS Laser Milling

Fig. 4 shows the micro-scale QR code generated by PS laser ablation. As the PS laser machined features had tapered side walls, the measurements of their widths were taken at the bottom of the protrusions representing the black squares/pixels in the QR code.

The average depths and widths of one pixel in the bitmap image of the “large” QR code are provided in Table 5. The table also includes the mean of the overall size of the QR code.

Table 5: “Large” QR Code Dimensions

Pixel Width (X) (µm)	**Pixel Width (Y) (µm)**	**Protrusions’ Height (µm)**	**Overall QR Code Width (X) (µm)**	**Overall QR Code Width (Y) (µm)**
Bottom	**Bottom**			
98.62 ± 6.12	98.83 ± 6.06	13.92 ± 1.06	2769.65 ± 167.26	2771.83 ± 166.78

It can be seen in Fig. 4 that the QR pattern was milled according to the scaled bitmap image and each pixel was textured with self-organised patterns. The average height of the PS laser milled fields, the white pixels of the QR-code, was estimated to be 13.92 µm (see Table 5) which differs from the targeted value of 10 µm, and also there was a draft angle on their walls. The functionality of the structured pattern, the QR code, can be affected by the dimensional accuracy of the milled square pockets but not by the depth variations and the surface texturing effects. However, the surface texturing might adversely affect the µIM process, in particular the part demoulding, if the textured fields represent a substantial part of the part surface area but this is not the case in the anti-counterfeiting applications.

The average widths at the top and the bottom of the measured QR pixels were 83.07 and 98.62 µm in the X direction and 83.04 and 98.83 µm in the Y direction, respectively (Table 5). The average pixel widths both at the top and bottom are considerably larger than the targeted values of 75 µm. Also, the overall average dimensions of the “large” QR code are bigger, 2.770 and 2.772 mm in X and Y directions respectively as stated in Table 5. These discrepancies are mostly due to not introducing a compensation of the beam diameter, 15 µm, in the laser milling strategies and also to some extent could be attributed to measurement errors as the edges of the QR code pixels are not well defined. It can also be seen in Fig 4 that some of the ablated material was re-deposited on the edges of the pockets/ pixels of the QR code that can lead to a further increase of the measurement uncertainty. Overall, these results are encouraging but they also show that further work is required to optimise the laser milling process and thus to improve the quality of the machined structures.

Finally in Fig 4b it can be observed that the pockets/pixels of the QR code were successfully textured with self-organised structures consisting of an array of relatively high aspect ratio micro holes with approximately 4.89 µm diameter. In addition, surface roughness measurements of the bottom / floor of the machined pockets were carried out using the Confocal Microscope and the Ra roughness value is 1.462 ± 0.06 µm.

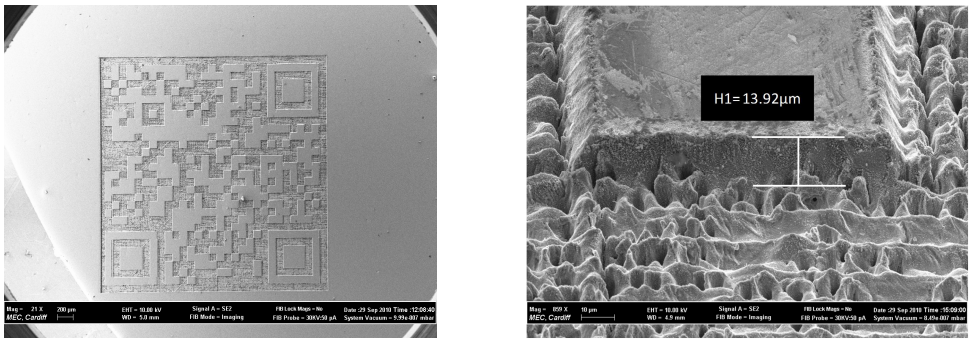

a) Overall view of micro-scale QR code b) A magnified image of the micro-scale QR Code

Fig. 4 Micro-scale QR code generated by PS laser ablation

4.1.2 NS Laser Milling

Table 6 reports the results of the surface roughness measurements after the NS laser machining of the 10x10 mm fields on samples 1, 2 and 3 that were measured using a sampling length of 0.8 mm and an evaluation length of 4 mm respectively in accordance with ISO 4288:1997 (ISO4288, 1997). Measurements were carried out diagonally across the machined fields to give the most accurate roughness measurement. The obtained average roughness values and the corresponding SEM images of the laser machined fields on samples 1, 2 and 3 are provided in Table 6.

Table 6 Average Surface Roughness Measurements of NS Laser Machined Fields.

Sample	Ra (µm)	Image of Machined Surface
1	0.22 ± 0.03	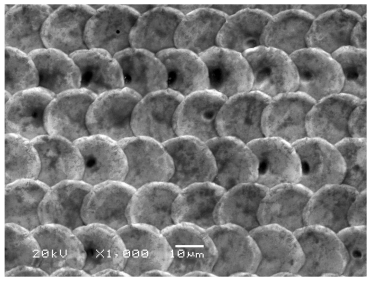
2	0.16 ± 0.01	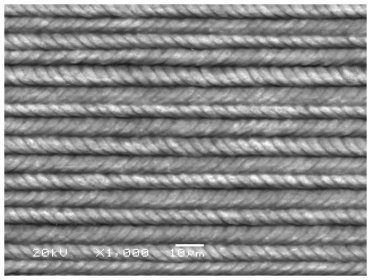
3	0.26 ± 0.03	

A comparison of the results in Table 6 shows that the best surface roughness, R_a value of 0.16 µm, is achieved on Sample 2. However, the surface roughness of all samples is comparable to that achievable after micro milling and thus can be considered acceptable for producing µIM tooling inserts. Thus, it is necessary to analyse the XRD results to determine whether NS laser ablation can be used as an alternative component technology to the PS laser ablation in the proposed process chain. Fig 5 shows the X-ray diffraction results of the as-received Vit 1b sample workpiece, sample 4, and after the NS laser machining of samples 1, 2 and 3. The typical broad diffraction maxima in the XRD pattern can be observed in Fig 5a that depicts the fully amorphous characteristics of the as-received Vit 1b sample. This is as expected and the XRD results are identical to those reported by other investigations of amorphous Zr-Ti-Ni-Cu-Be alloys (Waniuk, Schroers, & Johnson, 2003).

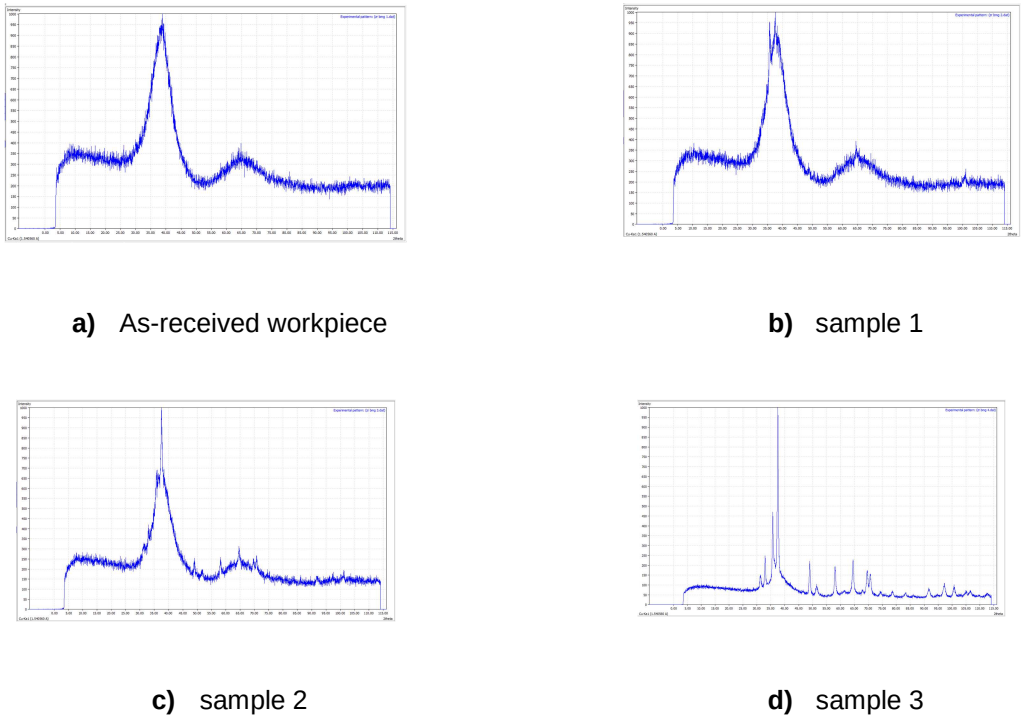

a) As-received workpiece **b)** sample 1

c) sample 2 **d)** sample 3

Fig 5 XRD Results for the As-received and Laser Machined Samples

In Figs 5b and 5c it can be observed that there are a few weak but sharp crystalline peaks superposing on the broad humps meaning that they are still predominantly amorphous. Whereas for

the sample 3 in Fig 5d there is a substantial increase in sharp crystalline peaks that indicates a substantial increase of the crystalline phase in the Vit 1b material. These results concur with those reported in another investigation where it was demonstrated that the non-crystalline morphology of a Mg-based BMG could be retained after optimising the NS laser ablation process (Lin et al., 2012). Thus, taking into account the surface roughness and XRD results obtained on the Vit 1b samples it can considered that after some further optimisation of the NS laser ablation process it will be possible to achieve the necessary micro machining response to potentially replace PS laser ablation in the proposed master making process chain.

4.2 FIB Milling

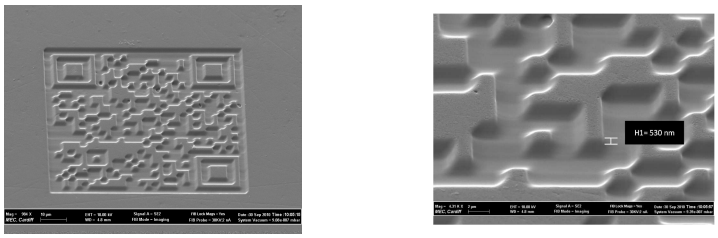

a) Overall view of Nano-scale QR code **b)** A magnified image of the nano-scale QR code

Fig 6 Nano-scale QR code generated by FIB milling

Fig. 6 shows the nano-scale QR code structure fabricated by FIB milling. It can be judged from this figure that the structure was milled satisfactorily on the BMG workpiece. Similarly to the results reported in the previous section, Table 7 presents the average values for the measured heights and widths of the smallest features. Also, Table 7 includes the average values of the QR code overall size.

From these measurement results it can also be seen that the average widths in the X and Y directions at the bottom of protrusions are larger than the nominal value of 2.59 µm. Again, this difference could be due to both not introducing a compensation for the beam diameter, 40nm during the FIB machining

and also due to measurement errors as the pixels' edges are rounded and difficult to locate precisely. Besides these two factors, the discrepancies could also be the result of calibration and set-up issues associated with the FIB system used. The table also includes the overall average width of the nano-scale QR code, 76.63 and 78.11 µm in X and Y directions, respectively. Taking into consideration these values and also that each side includes 29 pixels, it can be calculated that the average widths of the pixels in X and Y directions are 2.64 and 2.69 µm, respectively. These two values are very close to the nominal pixel size of 2.59 µm. Again, as it was the case with the bigger QR code, through some process optimisation, the FIB machining accuracy can be improved but nevertheless as it is, the nano-scale QR code has the required resolution to fulfil its functional requirements.

Table 7: "Small" QR Code Dimensions

Pixel Protrusion Width (X) (µm))	Pixel Protrusion Width (Y) (µm)	Protrusion Height (nm)	Overall QR Code Width (X) (µm)	Overall QR Code Width (Y) (µm)
Bottom	**Bottom**			
2.98 ± 0.21	3.09 ± 0.20	530.0 ± 71.1	76.63 ± 4.60	78.11 ± 4.69

The height measurements of the BMG insert are given in Table 7. It can be observed in Fig. 6b and Table 7, that the average height of the structures was estimated to be 530 nm while the specified target value was 900nm. Again, this result could be explained both with not calibrating the sputtering process, in particular the sputtering rate for the selected FIB milling parameters in Table 2, and also with the measurement errors associated with the quality of the "pixel" edges. An investigation of different factors that affect the accuracy of the FIB milling process was carried out in another research (Velkova, 2011). The findings of this study showed that the deviations in sizes of complex 3D structures could be kept within 2 to 5 % of their nominal dimensions by employing a specially developed methodology for optimising the layer-based FIB milling process. As this paper reports a feasibility study, the process settings were not optimised using this methodology. Thus, through such optimisation it will be possible to improve substantially the accuracy of the FIB milling process.

Finally, Fig. 6b shows that there is a draft angle on the vertical walls of the milled pockets. This phenomenon is due to the positional drift of the pattern during the FIB milling process that is caused

by relatively long machining times. As it can be judged from Fig. 7, the nano-scale QR code was successfully structured over the pre-existing micro topography created by PS laser milling. The alignment of the nano-scale pattern was performed using the approach described in the previous section and the positional error was estimated to be less than 2µm.

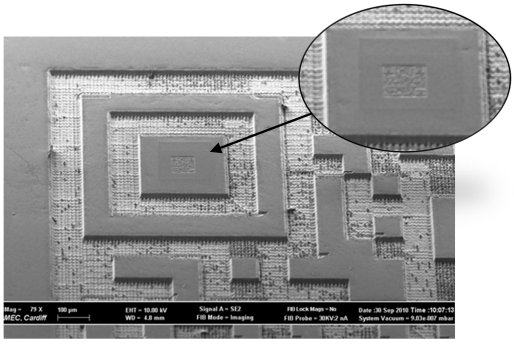

Fig. 7 Nano-scale QR code produced on the top of the micro-scale QR pattern

4.3. Micro-Injection Moulding

Utilising the BMG insert for µIM, polymer replicas in TOPAS 5013X (COC) were produced. Since the "small" QR code posed the greatest challenge, the replicated depths of the pattern were measured and compared for the five process settings in Table 4 and thus to determine the set of parameters which gave the best replication results. The surface topography was inspected using the SEM, whilst the instruments used to compare the QR code pattern depths were the AFM and the confocal microscope.

Figs 8a to 8f depict the SEM images of the polymer replicas produced with the five µIM process settings in Table 4, together with the corresponding AFM and confocal microscope surface inspection results. Studying the SEM images in Fig 8, it can be judged that the "small" QR code with sub-micron features was replicated satisfactorily. The best replication results were obtained with the higher mould temperatures of 130^{o}C and 140^{o}C. This is as expected because by increasing the mould temperature, the bulk temperature of the polymer can be kept sufficiently high to ensure the complete filling of the sub-micron surface structures (Griffiths et al., 2007; Tosello et al., 2010).

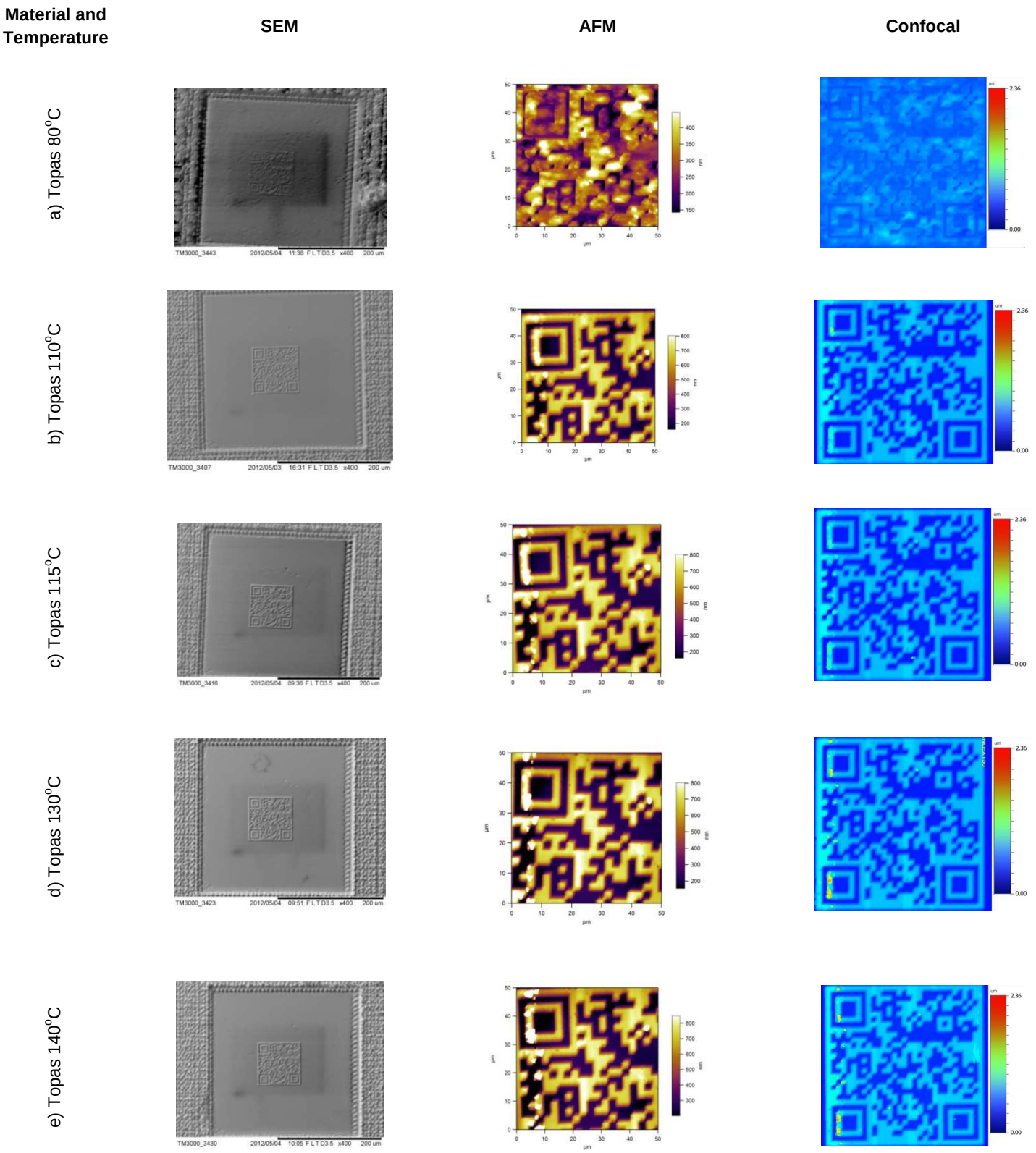

Fig 8 SEM images of µIM parts together with the AFM and Confocal Microscope surface inspection results

A histo-distribution generated from the AFM measurements of the inspected samples is presented in Fig 9 and concurs with the SEM surface analysis results. As can be observed in the figure the pattern height is much lower at the mould temperature of 80^{o}C. This is because the bulk temperature of the polymer cannot be kept sufficiently high and so the viscosity of the Topas 5013 melt remains relatively high, too. Consequently, the complete filling of the "small" QR code pattern cannot be achieved and thus resulting in premature solidification and incomplete filling of the small QR code features. From Fig. 9, it can also be observed that as the mould temperature increases progressively the polymer viscosity gets sufficiently low to fill the sub-micro features, and thus the cavities are filled much better. The best height replication results were obtained for the 130^{o}C and 140^{o}C mould temperature settings.

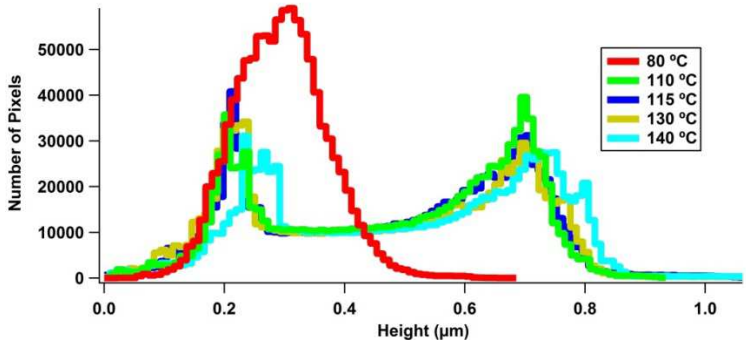

Fig 9 AFM Histo-distribution for the analysed polymer samples

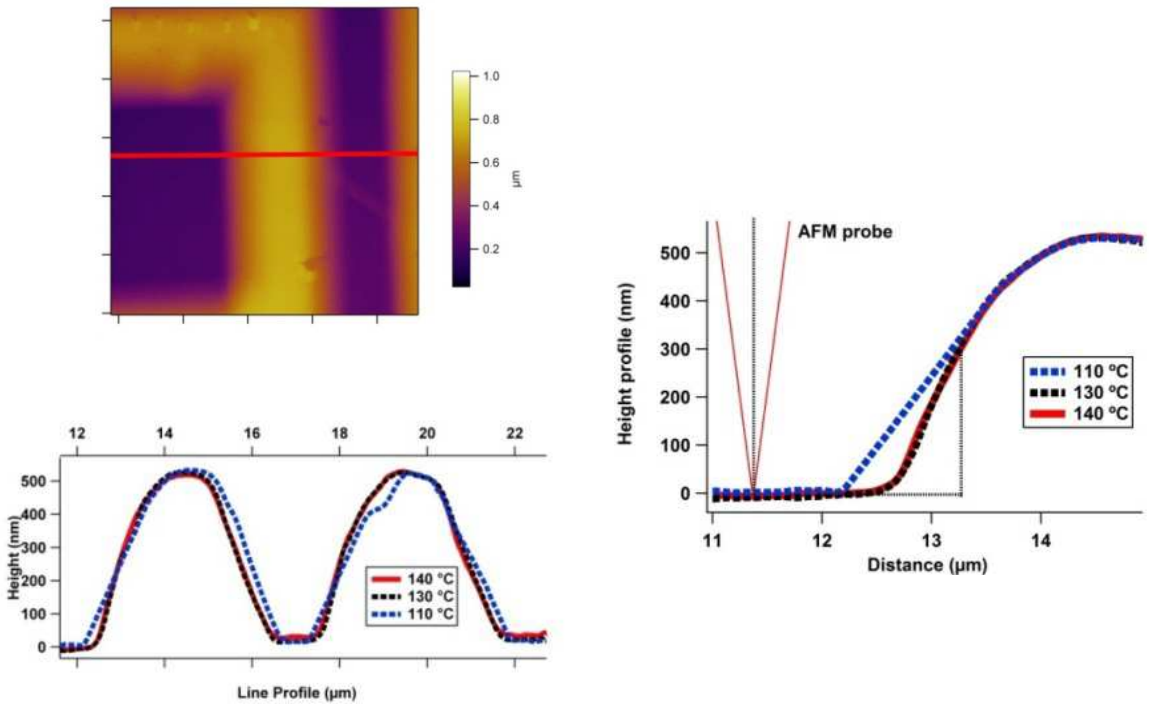

a) AFM Profiles of the top left feature

b) AFM Probe and Generated Profile

Fig. 10 Profiles of the top left feature of the "small" QR code

Based on the AFM scan data, a profile of the top left feature of the "small" QR code was generated. The profile is presented in Fig 10 and shows that the 130^{o} and 140^{o} C samples have sharper "pixel" edges then those at 110^{o}C. In addition, it can be observed that the feature depth is approximately 500 nm and this is in agreement with the confocal microscope results, below. The wall side angles of the QR grid are 37.2°, 37.2° and 16.6° for the samples produced at 140^{o}C, 130^{o}C and 110^{o}C, respectively. Figure 10b depicts the geometry of the AFM probe in relation to the line section of the QR grids for the 140^{o}C, 130^{o}C and 110^{o}C trials, respectively. As the angles are less than 60° the probe geometry did not affect the results. This shows again that the samples made at 130 and 140^{o}C are of better quality than those produced at 110^{o}C. Whilst the profiles of the 130^{o}C and 140^{o}C samples are virtually identical and steeper than the 110^{o}C sample, they still cannot be considered as edge-like. This is most likely due to the draft angle on the vertical walls of the FIB milled fields on the BMG insert and also possibly due to some trapped air in the mould. As suggested in literature the

latter problem could be potentially eliminated by air evacuation from the mould just before injection (Attia et al., 2009; Giboz et al., 2007).

An additional analysis to one of selected line sections of the insert and the polymer replicas for each of the 140^{o}C, 130^{o}C 115 ^{o}C, 110^{o}C and 80^{o}C µIM trials was carried out by using the confocal microscope data sets. In particular, the replication quality of the FIB structures on the replicas at these temperature settings was assessed by applying the methods for the Volume, Sa and Average Step height ratios as detailed in Section 3.6.3. The results are shown in Table 8.

Table 8: Results of Volume , Sa and Average Step Ratios for µIM Trials.

		Volume ratio	**Sa ratio**	**Step ratio**
Insert		1.000	1.000	1.000
Mould Temp (°C)	80	0.165	0.271	0.160
	110	0.821	0.921	0.928
	115	0.806	0.941	0.934
	130	0.913	0.956	0.945
	140	0.970	0.956	0.947

The best average step height ratios are 0.945 and 0.947 respectively, and they indicate that the 140^{o}C mouldings are marginally better than the ones produced at the mould temperature of 130^{o}C. Collectively, the best replication accuracy was obtained for the 130^{o} C and 140^{o}C mould temperature settings and this is in agreement with the results from the AFM inspection. It can also be observed in Table 8 that the Sa Ratio for both the 130^{o} C and 140^{o}C mould temperature trials is the same. Whilst, the volume ratios are 0.913 and 0.970 for the the130^{o} C and 140^{o}C mould temperature trials, respectively. The latter Volume Ratio indicates that a slightly better fill has been achieved for the 140^{o}C mould temperature setting than that obtained for the 130^{o}C trials. This analysis has showed clearly that the surface quality and the profiles of the replicated “small” QR codes were satisfactory for

the considered application. Therefore, given that the replication quality for 140^{o}C mould temperature setting are slightly better than that obtained at 130^{o}C, only the parts from the 140^{o} C trials were used to investigate further the replication fidelity for both the “large” and “small” QR codes.

4.3.1. “Large” QR Code

The “large” QR code produced by PS laser milling on the BMG insert was replicated well as far as it can be judged by comparing the image of the replica in Fig. 11 with the insert in Fig. 4.

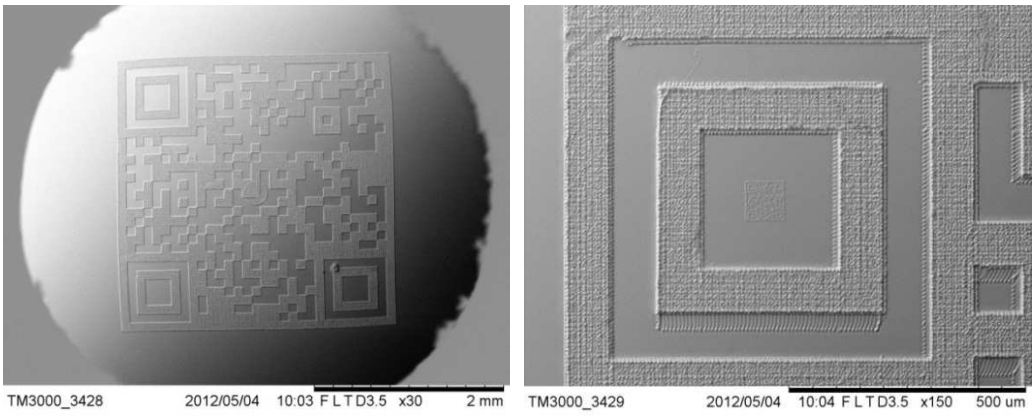

(a) (b)

Fig 11 : Replicated “large” QR Code (a) overall view (b) top left features of the code

The PS laser texturing of the “large” QR code white pixels was replicated successfully on the polymer parts as can be seen clearly in Fig 12 and “nub” structures with relatively high aspect ratio and an average diameter of 4.09 µm were created. This average value was calculated based on the confocal microscope inspections of three Topas parts. In addition, the average Ra surface roughness of the parts’ textured surfaces is 1.843 ± 0.41 µm. Comparing the diameters of the micro-holes and Ra values of the PS laser textured surfaces on the BMG insert with the diameters and Ra values of the replicated “nub” structures on the Topas parts, it can be judged that the texturing was replicated with relatively good fidelity. The use of BMG inserts for replicating such texturing effects on surfaces is

very important due to their very high wear resistance and thus being capable of retaining the surface functionality for more µIM cycles.

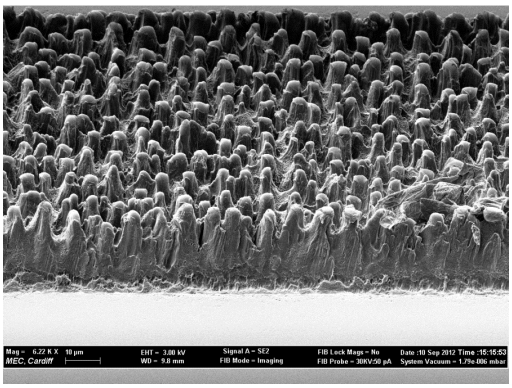

Fig 12 Surface texturing of the “large” QR Code replica

The results from the inspection of the smallest micro scale features of the “large” QR code replicas together with the average overall size of the code are provided in Table 9. If the dimensions of the pixels on the COC replicas and the BMG insert are compared in Tables 6 and 9 the deviation of the height is 3.52 % while for the width is 1.58% and 1.22% in the X and Y directions, respectively. These deviations are higher than the expected typical shrinkage values of 0.4 to 0.7% for this material but they could be explained both with some measurement errors and also the used injection moulding parameters which were not fully optimised.

The average width dimensions of the 29 “large” QR pattern’s pixels can also be calculated based on the overall size of the code in Tables 5 and 9. As stated before, these dimensions are likely to be more accurate estimates of the pixel sizes because the measurement error is “shared” between the pixels constituting the QR code. Thus, the average widths can be estimated to be 95.51 and 91.73 µm in the X direction and 95.58 and 91.64 µm in the Y direction for the BMG insert and the COC replicas, respectively. For the COC replicas, there is an average 5.7 µm difference with the as-measured pixel cavity values reported in Table 9 in particular 97.06 µm and 97.62 µm. This again can be explained with the measurement errors incurred whilst inspecting the individual pixels. Similarly, for the BMG insert, the average error between the estimated and the actual pixel sizes reported in Table 5 is approximately 3.18 µm. This means that the estimated average errors incurred when measuring the

overall size of the “large” QR code on the BMG insert and COC replicas are 3.18 µm and 5.7 µm respectively. If these two error values are taken into account in the shrinkage calculation, the average percentage difference between the overall side lengths of the replicated large QR code and the laser milled BMG QR code is approximately 4.13%. From a statistical point of view, using the paired-sample t test, it can be stated with 99% confidence that the difference between the means of the BMG insert and COC parts is significant and they can be predominantly attributed to shrinkage. In this case, the actual shrinkage is higher than the expected typical shrinkage values reported for this material. However, it should be noted that by subjecting the COC material to a high holding pressure should help minimise material shrinkage. In particular, one of the techniques that have been suggested to decrease the effect of shrinkage is to increase the holding pressure however this increases also the stresses inside the mouldings (Giboz et al., 2007).Thus, the results were not expected taking into account that a high holding pressure was used, 1300 bar, that is much higher than the recommended packing pressure for COC of 600 bar.

Overall, considering that this is only a feasibility study, and none of the component processes in the proposed chain have been fully optimised it can be stated that the “large” QR code was replicated with a relatively good fidelity. Also, it is clear that in order to produce a product with higher accuracy the laser machining and the micro-injection moulding stages in the process chain have to be optimised further and thus to improve the quality of replicated micro features. The analysis of the replication stage shows that the results can be affected significantly by the outcome of the preceding stages in the process chain, in particular the laser milling. Also, this feasibility study reveals some of the challenges in performing an effective dimensional quality control and reliable manufacturing when precise micro structures have to be produced.

Table 9: Replicated “large” QR code dimensions

Width (X) [µm]	**Width (Y) [µm]**	**Height [µm]**	**Overall Width (X) [µm]**	**Overall Width (Y) [µm]**
Top	**Top**			
97.06 ± 6.09	97.62 ± 5.94	13.43 ± 0.93	2660.03 ± 16 7.46	2657.65 ± 161.95

4.3.2. “Small” QR Code

Fig. 13 shows that the “small” QR code was replicated successfully on the COC parts. The average heights and widths of the smallest features together with the average overall size of the “small” QR code are provided in Table 10. If the dimensions of the smallest features on the COC replicas and the BMG insert are compared in Tables 7 and 10 the deviation of the height is 6.72 % while for the width is 3.36% and 6.15% in X and Y directions, respectively. Again, this is higher than the expected typical shrinkage values of 0.4 – 0.7% for this material. The average dimensions of the 29 “small” pixels was also calculated based on the overall size of the QR code in Tables 7 and 10, in particular the average widths were approximately 2.64 µm in the X direction and 2.69 µm in the Y directions for both the BMG insert and the COC replicas. Thus, the average errors incurred when measuring the overall size of the “small” QR code on the BMG insert and COC replicas is 0.37 µm and 0.225 µm respectively and it is mostly due to the edge definition as it is shown in Fig 14. If these two error values are taken into account in the shrinkage calculation, the measurement errors are much smaller, and the average percentage difference between the overall side lengths of the replicated “small” QR code and the FIB milled QR code on the BMG insert is approximately 0.05%.

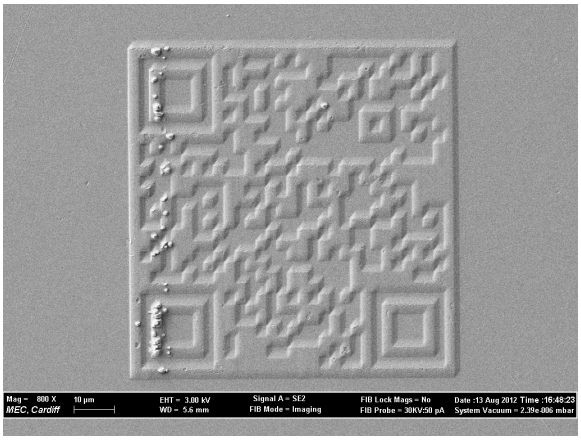

Fig 13 Replicated Small Scale QR Code.

From a statistical point of view, using the paired-sample t test, it can be judged with 80% confidence that there is a significant difference between the means of the small QR code overall side length of the BMG insert and the COC replicas. Therefore, it is not possible to state unequivocally if the observed difference is significant or whether it may be attributed to stochastic factors. This is reinforced even further when the magnitude of the measurement uncertainty is also taken into consideration with respect to the estimated percentage difference and the number of samples available.

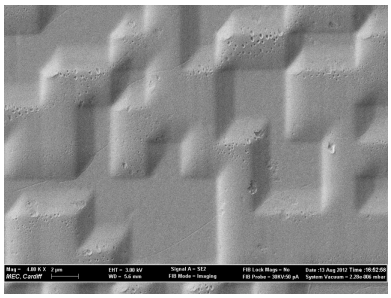

Fig 14 Feature edge quality of the replicated “small” QR code.

As stated above, in Tables 7 and 10, there is also a 6.72 % difference between the average height of the insert and the replicas that again could be attributed to the measurement errors, material shrinkage and not fully optimised replication process. Also, the research had revealed potential challenges in performing an effective dimensional quality control and reliable manufacturing at sub-micron scale.

Table 10 Replicated "small" QR code dimensions

Width (X) (μm)	Width (Y) (μm)	Height (nm)	Overall Width (X) (μm)	Overall Width (Y) (μm)
Top	**Top**			
2.88 ± 0.18	2.90 ± 0.18	494.4 ± 71.1	76.53 ± 4.60	78.00 ± 4.69

4.4. Future Research

The feasibility study highlighted that further research is necessary to address specific shortcomings in the proposed master making process chain. As it was already noted all component technologies in the proposed master-making process chain have to undergo further optimisation. Such process optimisation can be achieved either by employing specially developed methodologies such as that reported earlier for optimising the layer-based FIB milling process or through the use of DOE methodology. The DOE approach can be applied by conducting first screening experiments in order to identify critical control/input factors and also how their magnitude and direction affects the response variable(s); and' subsequently by employing response surface methodology to optimise the operation conditions (Clark, Horrell, Rogelstad, & Spagon, 1995; Montgomery, 2009).

The quality of the laser machined surfaces influences significantly the replication capabilities of the tools (Dobrev, Pham, & Dimov, 2005) and this was clearly seen in this research, too. After the μIM trials the BMG insert had traces of polymer adhering to the textured pixels as it is shown in Fig 15. . Thus, any laser texturing of inserts can lead to problems with the parts' demoulding if the surface area is relatively big and also to tool contamination as any polymer adhered to the mould will affect the replicas' quality. Thus, there is a need to optimise the laser machining process in order to ensure that any surface texturing or roughness does not cause problems during the replication stage. The NS laser machining results are very promising and demonstrate that the required surface quality for successful replication can be achieved. Taking into account the ablation mechanism when laser processing with ultra-short pulses is performed, it can be expected that an even better surface integrity than that reported for the NS laser ablation could be obtained after PS laser machining in

terms of surface roughness without changes in the non-crystalline morphology of the BMG workpiece. At the same time, it should be noted that the optimisation of the laser processing parameters will not be enough to produce sufficiently smooth surfaces for follow up FIB sub-micron and nano structuring.

This implies that additional surface conditioning and smoothening after the laser processing will be required. Recent results reported in the literature have shown that micro and nano scale features imprinted on Pt based BMGs may be erased by subsequent annealing in the BMG supercooled liquid region (Kumar & Schroers, 2008; Packard, Schroers, & Schuh, 2009) and thus to smooth the surface.

However, to make use of this process it is necessary to optimise it so that optimum annealing conditions for surface smoothening of Zr-based BMG masters are identified.

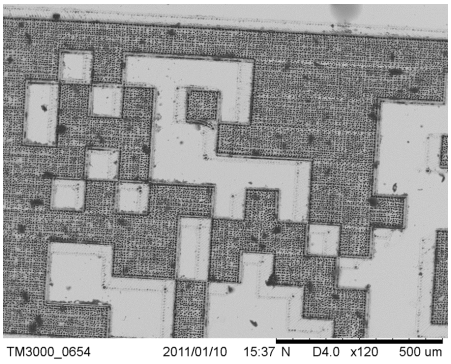

Fig. 15 Traces of polymer adherence on the BMG insert after µIM trials.

Finally, the replication results indicate that the Vit1B BMG is a promising candidate material for µIM master making. However, its durability and long term performance still need to be investigated before it can be considered as better alternative to the tooling grade steels used in both conventional and micro injection moulding. In particular, there is a need to assess the wear and fatigue performance of the Vit 1B BMG material when used in production runs.

5. Conclusions

A cost effective process chain for achieving FLSI in mass produced miniaturised devices was investigated in this feasibility study. It integrates compatible and complementary structuring and replication technologies by utilising a Zr-based BMG with very attractive mechanical properties. The capabilities of laser machining as a micro structuring technology were combined with those of the FIB milling to fabricate replication inserts incorporating micro and sub-micron structures. Then, to demonstrate the viability of the proposed master making process chain, the Zr-based BMG insert was integrated into a tool to produce a batch of thermoplastic parts by µIM.

The following conclusions about the proposed master making process chain and its component technologies could be drawn from this research.

- The NS laser machining showed that it is possible by proper selection of the processing settings to machine successfully Zr-based BMG workpieces with an acceptable surface integrity for µIM without triggering significant changes in the BMG short range atom arrangements. The results demonstrated that the required surface quality for successful replication can be achieved.
- With the selected PS laser processing parameters, it was possible to satisfactorily texture the BMG insert surface with high aspect ratio self-organised structures. Despite the fact that the selected PS laser machining parameters showed limitations with respect to the resulting structuring quality, it can be concluded that the PS laser process is a promising component technology for master making and also for achieving FLSI in replication tools.
- The viability of using Zr-based BMG masters to enable integration of compatible and complementary micro and sub-micron structuring and replication technologies for serial fabrication of FLSI thermoplastics components was demonstrated.
- The experimental investigation identified the factors affecting the performance of the proposed PS-FIB-µIM process chain. In particular, the following factors are considered to have the highest impact: the used process settings for its different component technologies, the Zr-based response to structuring technologies, e.g. PS Laser and FIB milling, with different specific processing

energies and the metrology issue in inspecting multi-scale structures. However, it was difficult to quantify their effects on the overall performance of the proposed process chain.

Collectively, the results demonstrate that there is good process compatibility and complementarity between the component technologies in the proposed process chain, especially for the length scale ranges aimed at this research. Such a process combination can therefore be used for the mass production of polymer parts incorporating different length scale features in one step. However, it is important to note that this is a feasibility study and thus it is necessary to investigate the proposed process chain further, in particular the PS laser and FIB milling processes, as master making technologies for producing replication inserts incorporating different length scale features. This includes further research into the specific process-material interactions of the considered component technologies and thus to identify their optimum processing windows in regards to the surface integrity and accuracy of the machined features/structures. Also, further NS laser process optimisation is required in order to achieve even better surface quality, whilst simultaneously preserving fully the non-crystalline morphology of the Zr-based BMG after the laser irradiation. Finally, further work is also required to optimise the µIM process in conjunction with the master making process chain and thus to improve further the quality of the replicated multi-scale structures, which was not the objective of this research.

ACKNOWLEDGMENTS

The research reported in this paper was funded by the FP7 programmes “Converging technologies for micro systems manufacturing” (COTECH)”, ‘‘Integrating European research infrastructures for the micro-nano fabrication of functional structures and devices out of a knowledge-based multimaterials’ repertoire” (EUMINAfab) and "High throughput integrated technologies for multimaterial functional micro components" (HINMICO), the UK Engineering and Physical Sciences Research Council (EP/F056745/1) and the Interreg IVB NWE project “ECO-efficient LASER technology for FACTories of the future” (ECO-LASEFACT).

The technical assistance of the authors' colleagues, particularly Dr. Ekaterin Minev, Dr. Petko Petkov, Dr. Samuel Bigot, Dr. Cristina L. Tuinea-Bobe and Dr. Colin Grant at Cardiff University and Bradford University, respectively, is also gratefully acknowledged.

References

(HLG), H. L. E. G. (2011). Key Enabling Technologies -- Final report. European Commission. Retrieved from <http://ec.europa.eu/enterprise/sectors/ict/files/kets/hlg_report_final_en.pdf>

Attia, U. M., Marson, S., & Alcock, J. R. (2009). Micro-injection moulding of polymer microfluidic devices. *Microfluidics and Nanofluidics*, *7*(1), 1–28. doi:10.1007/s10404-009-0421-x

Bigot, S., Minev, R., Dimov, S. S., & Dobrev, T. (2011). Function and length scale integration in innovative products - technical solutions and new organisational models. *International Journal of Manufacturing Technology and Management*, *23*(3/4), 157–178.

Bonse, J., Kruger, J., Hohm, S., & Rosenfeld, A. (2012). Femtosecond laser-induced periodic surface structures. *Journal of Laser Applications*, *24*, 4207–42006.

Brousseau, E. B., Dimov, S. S., & Pham, D. T. (2010). Some Recent Advances in Multi-Material Micro- and Nano-manufacturing. *International Journal of Advanced Manufacturing Technology*, *47*(1-4), 161–180.

Chen, C.-Y., Chung, C.-J., Wu, B.-H., Li, W.-L., Chien, C.-W., Wu, P.-H., & Cheng, C.-W. (2012). Microstructure and lubricating property of ultra-fast laser pulse textured silicon carbide seals. *Applied Physics A*, *107*(2), 345–350. doi:10.1007/s00339-012-6822-9

Clark, W., Horrell, K., Rogelstad, T., & Spagon, P. (1995). SEMATECH Qualification Plan Guidelines for Engineering. SEMATECH Inc.

Dimov, S. S., Brousseau, E. B., Minev, R., & Bigot, S. (2012). Micro- and nano-manufacturing: Challenges and opportunities. *Proc. Inst. Mechanical Engineers Part C: Journal of Mechanical Engineering Science*, *226*(3), 3–15.

Dobrev, T., Dimov, S. S., & Thomas, A. J. (2006). Laser milling: Modelling crater and surface formation. *Proceedings of the Institution of Mechanical Engineers, Part C: Journal of Mechanical Engineering Science*, *220*(11), 1685–1696. doi:10.1243/09544062jmes221

Dobrev, T., Pham, D. T., & Dimov, S. S. (2005). A simulation model for crater formation in laser milling. In W. Menz & S. S. Dimov (Eds.), *4M 2005 First International Conference on Multi-Material Manufacture Proceedings* (pp. 155–159). Karlsruhe: Elsevier.

Etsion, I. (2005). State of the Art in Laser Surface Texturing. *Transactions of ASME, Journal of Tribology*, *127*(1), 248–253.

Fadeeva, E., Truong, V. K., Stiesch, M., Chichkov, B. N., Crawford, R. J., Wang, J., & Ivanova, E. P. (2011). Bacterial Retention on Superhydrophobic Titanium Surfaces Fabricated by Femtosecond Laser Ablation. *Langmuir*, *27*(6), 3012–3019. doi:10.1021/la104607g

Fleischer, J., & Kotschenreuther, J. (2007). The manufacturing of micro molds by conventional and energy-assisted processes. *The International Journal of Advanced Manufacturing Technology*, *33*(1-2), 75–85. doi:10.1007/s00170-006-0596-1

Giboz, J., Copponnex, T., & Mele, P. (2007). Microinjection Moulding of Thermoplastic Polymers - A review. *Journal of Micromechanics and Microengineering*, *17*(6), R96 – R109.

Griffiths, C. A., Dimov, S. S., Brousseau, E. B., & Hoyle, R. T. (2007). The effects of tool surface quality in micro-injection moulding. *Journal of Materials Processing Technology*, *189*(1-3), 418–427.

Heckele, M., & Schomburg, W. K. (2004). Review on micro molding of thermoplastic polymers. *Journal of Micromechanics and Microengineering*, *14*(3), R1–R14. doi:10.1088/0960-1317/14/3/R01

Huang, C. K. (2007). Polymeric nanofeatures of 100 nm using injection moulding for replication. *Journal of Micromechanics and Microengineering*, *17*(8), 1518–1526.

Inoue, A. (2000). Stabilization of Metallic Supercooled Liquid and Bulk Amorphous Alloys. *Acta Materialia*, *48*, 278–306.

ISO4288. (1997). Geometrical Product Specifications (GPS) -- Surface texture: Profile method -- Rules and procedures for the assessment of surface texture.

Joint Committee for Guides in Metrology (JCGM). (2008). *Evaluation of measurement data — Guide to the expression of uncertainty in measurement (GUM)* (p. 121).

Kawasegi, N., Morita, N., Yamada, S., Takano, N., Oyama, T., Ashida, K., … Ofune, H. (2006). Rapid Nanopatterning of a Zr-based Metallic Glass Surface Utilizing Focused Ion Beam Induced Selective Etching. *Applied Physics Letters*, *89*(14), 143115–1431153.

Kirkup, L., & Frenkel, B. (2006). *An Introduction to Uncertainty in Measurement* (First.). Cambridge University Press.

Knowles, M., Kearsley, A., & Karnakis, D. (2007). INDUSTRIAL LASERS: Laser micromachining expands as technology develops. *Laser Focus World*. PennWell Corporation/Technology Group. Retrieved from http://www.laserfocusworld.com/articles/print/volume-43/issue-6/features/industrial-lasers-laser-micromachining-expands-as-technology-develops.html

Knowles, M. R. H., Rutterford, G., Karnakis, D., & Ferguson, A. (2007). Micro-machining of metals, ceramics and polymers using nanosecond lasers. *The International Journal of Advanced Manufacturing Technology*, *33*(1-2), 95–102. doi:10.1007/s00170-007-0967-2

Kumar, G., & Schroers, J. (2008). Write and erase mechanisms for bulk metallic glass. *Applied Physics Letters*, *92*(3), 31901–31903. doi:10.1063/1.2834712

Lalev, G., Dimov, S. S., Kettle, J., Van Delft, F., & Minev, R. (2008). Data Preparation for FIB machining of Complex 3D Structures. *Proc Instn Mech Engrs Part B: J Engineering Manufacture*, *222*(1), 67–76.

Lalev, G., Petkov, P., Sykes, N., Hirshy, H., Velkova, V., Dimov, S., & Barrow, D. (2009). Fabrication and validation of fused silica NIL templates incorporating different length scale features. *Microelectronic Engineering*, *86*(4-6), 705–708. doi:10.1016/j.mee.2009.01.074

Leach, R. K. (2001). Measurement Good Practice Guide No. 37 -- The Measurement of Surface Texture using Stylus Instruments. (N. P. Laboratory, Ed.).

Li, W., Minev, R., Dimov, S. S., & Lalev, G. (2007). Patterning of Amorphous and Polycrystalline Ni78B14Si8 with a Focused Ion Beam. *Applied Surface Science*, *253*(12), 5404–5410.

Lin, H.-K., Lee, C.-J., Hu, T.-T., Li, C.-H., & Huang, J. C. (2012). Pulsed laser micromachining of Mg-Cu-Gd bulk metallic glass. *Optics and Lasers in Engineering*, *50*(6), 883–886. doi:http://dx.doi.org/10.1016/j.optlaseng.2012.01.003

Loffler, J. F., Kundig, A. A., & Dalla Torre, F. H. (2007). Rapid Solification and Bulk Metallic Glasses --- Processing and Properties. In J. R. Groza, J. F. Shackelford, E. J. Lavernia, & M. T. Powers (Eds.), *Materials Processing Handbook* (pp. 17–44). CRC Press.

Minev, R., Ilieva, M., Kettle, J., Lalev, G., Dimov, S. S., Tzaneva, D., … Shishkov, R. (2010). Deposition and FIB Milling of Anticorrosive CrC Coatings on Tool Steel Substrates. *International Journal of Advanced Manufacturing Technology*, *47*(1-4), 29–35. Retrieved from http://dx.doi.org/10.1007/s00170-009-2078-8, 2008

Minev, R., Vella, P. C., Brousseau, E. B., Dimov, S. S., Minev, E., & Matthews, C. W. (2010). Methodology for Capability Maturity Assessment of MNT Chains. In B. Fillon, C. Khan-Malek, & S. S. Dimov (Eds.), *7th International Conference on Multi-Material Micro Manufacture* (pp. 249–252). Bourg en Bresse and Onayonnax, France: Research Publishing.

Minev, R., Vella, P. C., Brousseau, E. B., Dimov, S. S., Scholz, S., & Matthews, C. W. (2010). Capability Maturity Study of the Horizontal and Vertical Integration of Structuring, Patterning and Characterization of MNTs. In B. Fillon, C. Khan-Malek, & S. S. Dimov (Eds.), *7th International Conference on Multi-Material Micro Manufacture* (pp. 253–256). Bourg en Bresse and Oyonnax, France: Research Publishing.

Monkkonen, K., Hietala, J., Paakkonen, P., Paakkonen, E. J., Kaikuranta, T., Pakkanen, T. T., & Jaaskelainen, T. (2002). Replication of Sub-Micron Features Using Amorphous Thermoplastics. *Polymer Engineering and Science*, *42*(7), 1600–1608.

Montgomery, D. C. (2009). *Design and Analysis of Experiments* (7th Editio., p. 656). John Wiley & Sons Inc.

Nayak, B. K., & Gupta, M. C. (2010). Self-organized micro/nano structures in metal surfaces by ultrafast laser irradiation. *Optics and Lasers in Engineering*, *48*(10), 940–949. doi:http://dx.doi.org/10.1016/j.optlaseng.2010.04.010

Packard, C. E., Schroers, J., & Schuh, C. A. (2009). In situ measurements of surface tension-driven shape recovery in a metallic glass. *Scripta Materialia*, *60*(12), 1145–1148. doi:http://dx.doi.org/10.1016/j.scriptamat.2009.02.056

Petkov, P. V, Dimov, S. S., Minev, R. M., & Pham, D. T. (2008). Laser milling: Pulse duration effects on surface integrity. *Proceedings of the Institution of Mechanical Engineers, Part B: Journal of Engineering Manufacture*, *222*(1), 35–45. doi:10.1243/09544054jem840

Petkov, P. V, Scholz, S., & Dimov, S. S. (2008). Strategies for material removal in laser milling. In S. S. Dimov & W. Menz (Eds.), *4M 2008 - Fourth International Conference on Multi-Material Micro Manufacture Proceedings* (pp. 249–252). Cardiff, Wales, UK: Whittles Publishing.

Pham, D. T., Dimov, S. S., Ji, C., Petkov, P. V, & Dobrev, T. (2004). Laser milling as a `rapid micromanufacturing process . *Proc. Instn Mech. Engrs Part B: J. Engineering Manufacture* , *218*, 1–7.

Pham, D. T., Dimov, S. S., & Petkov, P. V. (2007). Laser Milling of Ceramic Components. *International Journal of Machine Tools & Manufacture 47 (2007) 618–626*, (47), 618–626.

Platzgummer, E., Loeschner, H., & Gross, G. (2008). Projection Maskless Patterning for Nanotechnology Applications. In *52nd International Conference on Electron, Ion and Photon Beam Technology and Nanofabrication* (pp. 2059–2063). AVS.

Quintana, I., Dobrev, T., Aranzabe, A., Lalev, G., & Dimov, S. S. (2009). Investigation of Amorphous and Crystalline Ni Alloys Response to Machining with Micro-second and Pico-second Lasers. *Applied Surface Science*, *255*(13-14), 6641–6646.

Scholz, S. G., Griffiths, C. a., Dimov, S. S., Brousseau, E. B., Lalev, G., & Petkov, P. (2011). Manufacturing routes for replicating micro and nano surface structures with bio-mimetic applications. *CIRP Journal of Manufacturing Science and Technology*, *4*(4), 347–356. doi:10.1016/j.cirpj.2011.05.004

Scholz, S., Griffiths, C. A., Dimov, S. S., Brousseau, E. B., Lalev, G., & Petkov, P. V. (2009). New Process Chains for Replicating Micro and Nano Structured Surfaces with Bio-mimetic Applications. In *ANTEC 2009 - Proceedings of the 67th Annual Technical Conference & Exhibition* (pp. 3021–3027). Chicago.

Sha, B., Dimov, S., Griffiths, C., & Packianather, M. S. (2006). Micro-injection moulding: Factors affecting the achievable aspect ratios. *The International Journal of Advanced Manufacturing Technology*, *33*(1-2), 147–156. doi:10.1007/s00170-006-0579-2

Svintsov, A., Zaitsev, S., Lalev, G., Dimov, S. S., Velkova, V., & Hirshy, H. (2009). FIB sputtering optimization using Ion Reverse Software. *Microelectronic Engineering*, *86*(4-6), 544–547. doi:http://dx.doi.org/10.1016/j.mee.2009.01.073

Tosello, G. (2008). *Precision Moulding of Polymer Micro Components - Optimistation, Simulation , Tooling, Quality Control and Multi-material Application*. DTU.

Tosello, G., Bissacco, G., Tang, P. T., Hansen, H. N., & Nielsen, P. C. (2008). High Aspect Ratio Micro Tool Manufacturing for Polymer Replication using µEDM of Silicon, Selective Etching and Electroforming . *Micosyetem Technologies*, *14*(9-11), 1757–1764.

Tosello, G., & Chiffre, L. De. (2004). *Standard Traceability and Measurement Uncertainty* (p. 116).

Tosello, G., Gava, A., Hansen, H. N., & Lucchetta, G. (2010). Study of process parameters effect on the filling phase of micro-injection moulding using weld lines as flow markers. *International Journal of Advanced Manufacturing Technology*, *47*, 81–97.

Tosello, G., Hansen, H. N., & Gasparin, S. (2009). Applications of dimensional micro metrology to the product and process quality control in manufacturing of precision polymer micro components. *CIRP Annals - Manufacturing Technology*, *58*(1), 467–472. doi:10.1016/j.cirp.2009.03.027

Tosello, G., Marinello, F., & Hansen, H. N. (2012). Characterisation and analysis of microchannels and submicrometre surface roughness of injection moulded microfluidic systems using optical metrology. *Plastics, Rubber and Composites*, *41*(1), 29–39. doi:10.1179/0743289811Y.0000000017

United Kingdom Accreditation Service (UKAS). (2007). *The Expression of Uncertainty and Confidence in Measurement* (Vol. 44, pp. 1 – 82).

Uriarte, L., Herrero, a, Ivanov, a, Oosterling, H., Staemmler, L., Tang, P. T., & Allen, D. (2006). Comparison between microfabrication technologies for metal tooling. *Proceedings of the Institution of Mechanical Engineers, Part C: Journal of Mechanical Engineering Science*, *220*(11), 1665–1676. doi:10.1243/09544062JMES220

Vehse, M., Lobler, M., Schmitz, K. P., & Seitz, H. (2012). Laser induced surface structure on stainless steel influences cell viability. *Biomed Tech*, *57*(Suppl. 1), 419–421.

Velkova, V. (2011). *Focused Ion Beam Technology: Implementation in Manufacturing Platforms and Process Optimisation*. *Manufacturing Engineering Centre, School of Engineering,*. Cardiff University, Cardiff.

Velkova, V., Lalev, G., Hirshy, H., Omar, F., Scholz, S., Minev, E., & Dimov, S. (2011). Process chain for serial manufacture of 3D micro- and nano-scale structures. *CIRP Journal of Manufacturing Science and Technology*, *4*(4), 340–346. doi:10.1016/j.cirpj.2011.03.005

Velkova, V., Lalev, G., Hirshy, H., Scholz, S., Hiitola-Keinänen, J., Gold, H., … Dimov, S. (2010). Design and validation of a novel master-making process chain for organic and large area electronics on flexible substrates. *Microelectronic Engineering*, *87*(11), 2139–2145. doi:10.1016/j.mee.2010.01.015

Vella, P. C., Brousseau, E. B., Minev, R., & Dimov, S. S. (2010). A Methodology for Technology Maturity Assessment of Micro and Nano Manufacturing Processes and Process Chains. In F. E. Pfefferkorn (Ed.), *The 5th International Conference on MicroManufacturing (ICOMM/4M 2010)* (pp. 327–334). Madison, Wisconsin, USA.

Wang, X., Lu, P., Dai, N., Li, Y., Liao, C., Zheng, Q., & Liu, L. (2007). Noncrystalline Micromachining of Amorphous Alloys Using Femtosecond Laser Pulses. *Materials Letters*, *61*(21), 4290–4293.

Waniuk, T., Schroers, J., & Johnson, W. L. (2003). Timescales of crystallization and viscous flow of the bulk glass-forming Zr-Ti-Ni-Cu-Be alloys. *Physical Review B*, *67*(18), 184203–184209. Retrieved from http://link.aps.org/doi/10.1103/PhysRevB.67.184203

Wu, B., & Ozel, T. (2011). Micro-Laser Processing. In M. Koc & T. Ozel (Eds.), *Micro-Manufacturing -- Design and Manufacturing of Micro-Products* (First., pp. 159–195). Wiley.

Wu, P. H., Cheng, C. W., Chang, C. P., Wu, T. M., & Wang, J. K. (2011). Fabrication of large-area hydrophobic surfaces with femtosecond-laser-structured molds. *Journal of Micromechanics and Microengineering*, *21*(11), 115032.

Youn, S. W., Takahashi, M., Goto, H., & Maeda, R. (2006). Microstructuring of glassy carbon mold for glass embossing -- Comparison of focused ion beam, nano/femtosecond-pulsed laser and mechanical machining. *Microelectronic Engineering*, *83*(11- 12), 2482–2492. doi:http://dx.doi.org/10.1016/j.mee.2006.05.007

Zhang, G., Liu, Y., & Zhang, B. (2006). Effect of Annealing Close to Tg on Notch Fracture Toughness of Pd-based Thin-film Metallic Glass for MEMS Applications. *Scripta Materialia*, *54*(5), 897–901.